A COMPARISON OF PERFORMANCE BETWEEN UAV AND SATELITE IMAGERY FOR N STATUS ASSESSMENT IN CORN

N. Tremblay, P. Vigneault, C. Bélec and E. Fallon

Horticulture Research and Development Centre
Agriculture and Agri-Food Canada
St-Jean-sur-Richelieu, QC, Canada

M.Y. Bouroubi

Effigis Geo Solutions
Montreal, QC, Canada

ABSTRACT

For the sensing of crop conditions, a number of platforms, varying from proximal (tractor-mounted) ones to satellites orbiting the Earth, are available. Access to unmanned aerial vehicles (UAVs), or drones, that are able to carry sensors payloads providing data at a very high spatial resolution has recently aroused a great deal of interest. This study compares performance between UAV imagery acquired in a corn nitrogen (N) response trial set-up. The nitrogen (N) response trial consisted of two fields (one loamy, one clayey) sowed on two different dates at Agriculture and Agri -Food Canada's L'Acadie Experimental Farm, in the Montérégie region of Quebec, Canada. Eight unreplicated N treatment rates (from 0 to 200 kg N ha^{-1}) were applied, with or without irrigation, to create a gradient of crop development stages and N status at the time of imagery acquisition. Multispectral imagery from the Pléiades-1B satellite was acquired on 8 July 2013. Then, 4 d later, a multispectral image was acquired with a UAV responder. On the day of UAV imagery acquisition, a ground-truthing campaign was performed. Leaf area index (LAI), chlorophyllmeter (with a SPAD chlorophyll meter), and destructive biomass data were measured at 96 points. The Soil-Adjusted Vegetation Index (SAVI) was calculated for both the Pléiades-1B and the UAV images and was matched to the ground-truthing database to perform the statistical comparisons. Relationships were established between the SAVI and the LAI, SPAD chlorophyll and biomass biophysical descriptors measured on the ground for both the satellite and the UAV imagery. The SAVI acquired from a UAV was better correlated than imagery from a satellite to fresh biomass ($R^2 = 0.93$ for the UAV vs 0.88 for the satellite) and to LAI ($R^2 = 0.91$ for the UAV vs 0.74 for the satellite). Image segmentation on the UAV imagery improved R^2 by only 0.02 to 0.03 points. The accurate remote estimation of chlorophyll status from a corn crop at an early growth stage remains a challenge, even with pure leaf endmembers resulting from image segmentation, because of relatively low and more variable LAI values at that stage than at a later ones. The finer spatial resolution provided by the UAV allowed the observation of drainage effects on the vegetation, which were not clearly visible in the satellite image.

INTRODUCTION

The recent introduction of unmanned aerial vehicle (UAV) platforms offers an additional option for crop sensing. Their interest lies in fast deployment, very high spatial resolution and the opportunity to customize the imaging payload to suit the spectral requirements of the mission. Zarco-Tejada et al. (2012) were able to measure chlorophyll fluorescence and other biophysical descriptors of vegetation from a UAV carrying a thermal and a hyperspectral detector. Rey et al. (2013) reported that multispectral UAV imagery correlated to vine vigor and yield parameters and that the images required very complex processing to be useful for quantitative measurement. Smaller pixel sizes offer a very detailed visual description of the field. They make it possible to determine the precise location of rows and plants at early stages in the growing season, a time when it is still possible to act with management practices or corrective measures in tall crops such as corn. Hunt et al. (2013) summarized the problems and opportunities related to UAV sensing for quantitative measurements in crop assessment. Those authors suggested that downscaling by averaging pixel values does not take advantage of the existence of pure endmembers of leaves, soil and shadow in a very high-spatial-resolution image. Indeed, smaller pixel sizes offer the opportunity to apply segmentation procedures that purify spectral information from vegetation and separate it from background information. Zhang and Kovacs (2012) produced a detailed review of UAV use and its potential and limitations in precision agriculture. Laliberte et al. (2011) compared the spectral response of vegetation and soil from the WorldView-2 satellite and a multispectral MCA-6 camera (Tetracam, Inc. Chatsworth, CA) on board a UAV. The images were acquired 2 wk apart. The correlation of reflectance measurements ranged from R^2 values of 0.57 to 0.97 but tended to be higher for vegetation targets.

Although a certain degree of correspondence can be expected between UAV and satellite imagery, their respective performance for precision farming has never been directly assessed on images at close acquisition dates (4 d apart). The objective of this study was to examine if the higher spatial resolution (±25 cm) provided by a UAV offers a significant advantage over high resolution satellite imagery (2-m resolution) for the characterization of vegetation indices and biophysical descriptors (biomass, leaf area index [LAI], and chlorophyll) of a corn crop at an early stage.

MATERIALS AND METHODS

Field site and experimental design

The experiment was conducted in the summer of 2013 on corn (*Zea mays* L.). The fields, named as 56-64 and 58-66, were located at the L'Acadie Experimental Farm, Quebec, Canada (45°17′43.30″N, 73°20′47.70″W). The fields were characterized mainly by loams and clay loams of the Laprairie and Sabrevoix series, and by clay loams of the Bearbrook and St.Laurent series (Lamontagne et al., 2001). These series are in the Typic Humaquepts subgroup. The fields were relatively flat, and the apparent soil electrical conductivity (EC_a) measurements showed moderate variability from 3 to 10 10 mS m^{-1} at shallow depth, as measured with a VERIS model 3100 sensor cart system (Veris Technologies, Salina, KS).

Table 1. Description of the experimental design

	Field 56-64				Field 58-66			
Dominant soil texture	clay-loam				loam			
date of soil apparent electrical conductivity	18 October 2009							
block dimension (m)	50 × 15							
plot dimension (m)	6 × 15							
corn variety	Pioneer 38M58 (2800 CHU†)							
sowing number#	1		2		1		2	
date of sowing	30 Ap.		5 June		30 Ap.		5 June	
irrigations	Yes	No	Yes	No	Yes	No	Yes	No
numbers of plots	8	8	8	8	8	8	8	8
In-season N app. (side-dress at V5-6‡)	18 June		9 July		18 June		9 July	
date of irrigation #1	21 June	n/a	21 June	n/a	21 June	n/a	21 June	n/a
date of irrigation #2	5 July	n/a	5 July	n/a	5 July	n/a	5 July	n/a
date of irrigation #3	15 July	n/a	15 July	n/a	15 July	n/a	15 July	n/a
date of satellite imagery acquisition	8 July							
date of UAV imagery acquisition	11 July							

† CHU, crop heat units.
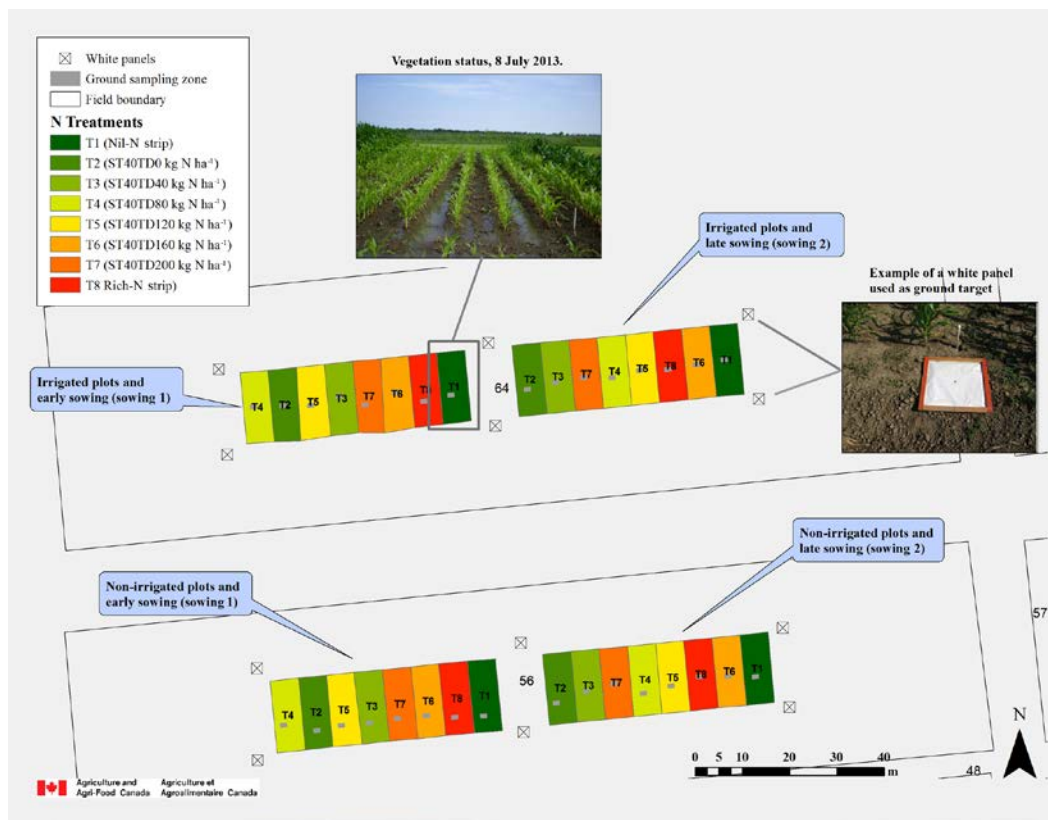‡Growth stage as defined by Ritchie et al. (1996).

Figure 1. Experimental design and ground-truthing sampling locations (example for Field 56-64).

Eight in-season nitrogen (N)-rate treatments plots (including no nitrogen or Nil-N, and non-limiting N fertilizer applications or Rich-N) were randomized within four blocks for each of the two dominant soil textures. At sowing, all plots except the Nil-N one received 40 kg N ha^{-1} banded (starter-N). The Rich-N plots also received 200 kg N ha^{-1} broadcast before sowing. At the time of in-season N application (Table 1), the N-rate treatments were 40, 80, 120, 160 and 180 kg N ha^{-1}, on top of the starter-N application. Figure 1 shows how the treatments were laid out in Field 58-66. The fields were under conventional tillage with a row spacing of 0.75 m. One irrigation sprinkler line was established transversally in the middle of two of the four blocks (Fig. 1). This irrigation set-up was expected to produce a spatially variable water supply as the amount of water normally decreases as the distance from the sprinkler heads increases. The actual spatial distribution of the applied irrigation water was measured by a network of pluviometers corresponding to the sampling points. Table 1 shows all the details and field characteristics.

Ground truthing

Two ground-truthing campaigns were conducted during the season. The first campaign took place during satellite image acquisition (Table 1) at side-dressing, covering only the Sowing 2 (late sowing) block area (total of 32 points). The second campaign was aligned with UAV image acquisition and covered all the

plots (total of 64 points). These points were also used to analyse the satellite image since only 4 d separated the two campaigns.

Each sampling point was randomly selected and positioned with a RTK (real-time kinematic) GPS receiver (SXBlue-IIIL; Geneq Inc., Montreal, QC, Canada) that is accurate to 5 cm). Figure 1 shows the distribution of the ground-truthing sampling points in Field 58-66 (see the grey rectangle within each plot, corresponding at the exact surface of measurement). Some plots had two sampling points (data not shown); therefore, a radius of at least 2 m was left between the two sampling points as well as between plot boundaries. Corresponding LAI measurements were take with a LAI-2200 instrument (Li-Cor inc., Lincoln, NE), and chlorophyll levels were estimated using a SPAD-502 chlorophyllmeter (Konica Minolta Camera Co., Ltd., Osaka, Japan). Fresh biomass was sampled, weighed and used to correlate with remote sensing parameters. Lastly, a database was created to superpose all the measurement values as the pixel values extracted from the satellite and the UAV imagery.

Image acquisition

Mini-MCA

A multispectral camera (Mini-MCA, Tetracam inc., Chatsworth, CA) was used to acquire images at very high spatial resolution (<25 cm). The camera provided six spectral bands (450, 550, 650, 700, 740 and 850 nm) from the blue to the near-infrared (NIR). The charge-coupled device counted 1.3 megapixels with an 8bit unsigned radiometric precision. Figure 2 shows the filter sensitivity for each of the six bands (the sensitivity was carefully chosen in order to reduce the influence of the atmospheric gases transmittance). The camera was carried by a responder-type UAV (http://ingrobotic.com/aircrafts/rotorcraft-responder/) operated by ING Robotic Aviation (Sherbrooke, QC, Canada) (Fig. 3). The campaign was performed on 11 July (Table 1) at the end of the afternoon (between 3 and 4 PM) under a clear sky with winds less than 15 km h^{-1}, at an altitude of around 244 m. White panels (0.50 × 0.50 m) had previously been installed on the ground and GPS-located for image georeferencing. The responder has a 25-min flying time. Its payload can reach 12 kg and the radio line of sight from the operator is 10 km.

To transform the pixel numeric value into a ground reflectance value, two radiometric corrections were applied, as follows. (1) Since it was necessary to reduce the "vignetting" effect, which was high in this case owing to the UAV's low altitudes of acquisition (150 to 250 m), a "geometric-optic" model based on the relationship $DN_{corr} = DN_{ori} \cdot (\cos\theta)^4$ was used, where DN_{corr} is the new digital numbers from the corrected image, DN_{ori} is the digital numbers of the uncorrected image, and θ is the viewing angle calculated for each pixel of the image. (2) Surface reflectance was estimated, as required when multispectral data are used to estimate biophysical parameters. The image corrected for vignetting was transformed into ground reflectances using the simple model $Refl = a\, DN_{corr} + b$. The parameters a and b were estimated by considering samples of pixels in surfaces (trees, bare soil, gravel) of known reflectances found in the ASTER spectral library. All the operations were performed in MATLAB (MathWorks, Natick, MA) and Geomatica (PCI Geomatics, Richmond Hill, ON, Canada).
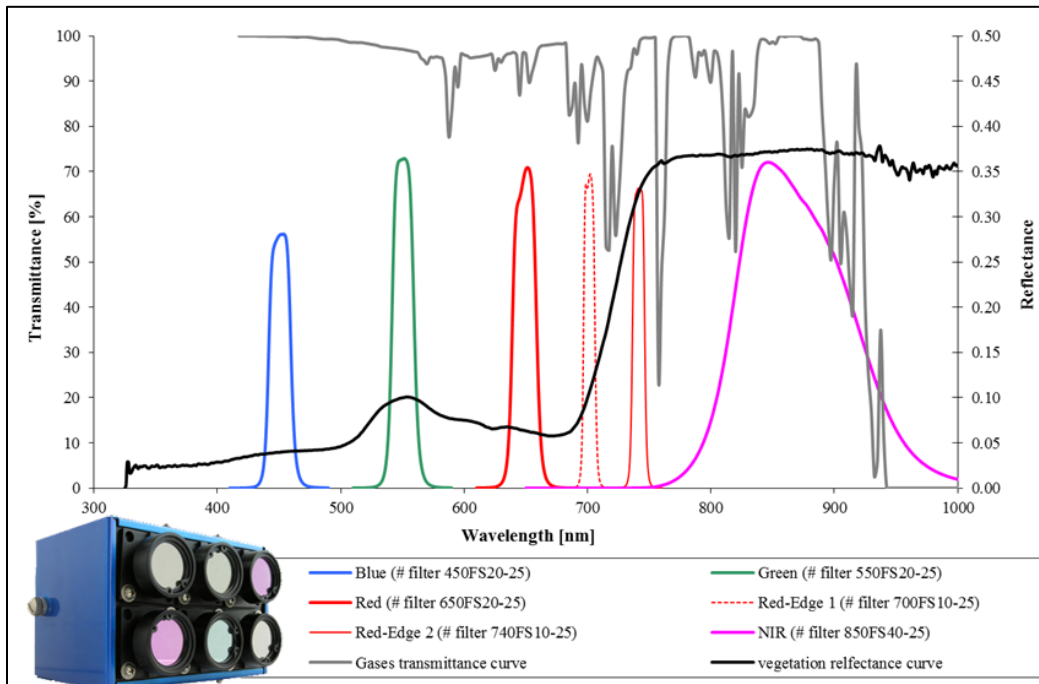
Figure 2. Mini-MCA camera configuration and sensitivity of the bandpass filters for each band versus atmospheric transmittance and the standard vegetation reflectance curve.

Figure 3. Picture of the responder and its payload.

Pléiades-1B

A satellite image from the Pléiades-1B sensor (Astrium, Toulouse, France) was acquired on 8 July 2013 at around 11 AM. The image covered more than 100 km^2 and was considered to be high quality with 0% cloud cover. The image presented panchromatic features (0.5 m; 470 to 830 nm) and multispectral features (2 m, R+G+B+NIR; 430 to 940 nm). Ground reflectance was estimated from the Pléiades-1B images using REFLECT radiative transfer model (Bouroubi

et al., 2010) in three steps: (1) sensor calibration, where apparent radiance (L^{sat}) was calculated from digital numbers (DN) using calibration coefficients given in the auxiliary files; (2) calculation of apparent reflectance (ρ^{sat}) by dividing L^{sat} by the radiance of a Lambertian target with unit reflectance given by $(E_0.\cos\theta_s)/\pi$, where E_0 is the solar radiation at the top of the atmosphere and θ_s the solar zenith angle; and (3) calculation of ground reflectance using the formula $\rho_G = T \rho^{sat} + L_{atm}$, where the atmospheric parameters T (transmittance) and L_{atm} (path radiance) are calculated using the routines of the 6S atmospheric code that estimates gaseous and aerosol scattering and gaseous absorption from meteorological inputs (mainly aerosol optical depth and water vapor content).

Calculation of the vegetation indices

Three vegetation indices were used for this study. The Soil-Adjusted Vegetation Index (SAVI), (Huete, 1988) and the Optimized Soil-Adjusted Vegetation Index (OSAVI), (Rondeaux et al., 1996) were selected because of their ease of use in the context of operational observations on agricultural landscapes and because they reduce the effect of soil (Haboudane et al., 2002). The third vegetation index used in this study was the ratio of the Transformed Chlorophyll Absorption in Reflectance Index (TCARI) to the OSAVI (Haboudane et al., 2002) which was shown to remove LAI influence on chlorophyll estimates. All the vegetation indices were calculated, using Geomatica, from the reflectance values of the imagery presented in this paper. Mapping and merging with the sampling point database were done with the ArcGIS software suite (ESRI, Redlands, CA).

Creation of an accurate database

The small size of the total scene and the flight altitude obviated the need to mosaic the images from the Mini-MCA/UAV system. The aim of the campaign was to cover all experimental units in a single soil type in one shot. The two resulting images were post-treated separately.

To compare the images with the ground-truthing data, an average pixel value was calculated from all pixels contained in the 1.5×1.0 m sampling area (Fig. 4A). The results were integrated in the database. For the Pléiades-1B image (2 m resolution), an average of the pixels involved in the sampling area was calculated.

RESULTS AND DISCUSSION

There was a highly significant linear relationship ($R^2 = 0.88$) between the SAVI estimates from the Pléiades-1B satellite and those from the Mini-MCA camera (Fig. 5), within the range of correlation reported by Laliberte et al. (2011). SAVI estimates were generally higher with the Mini-MCA possibly owing to the later acquisition with that device (4 additional days of growth) and to the fact that pixels in the Pléiades-1B image contain more soil that Mini-MCA pixels.
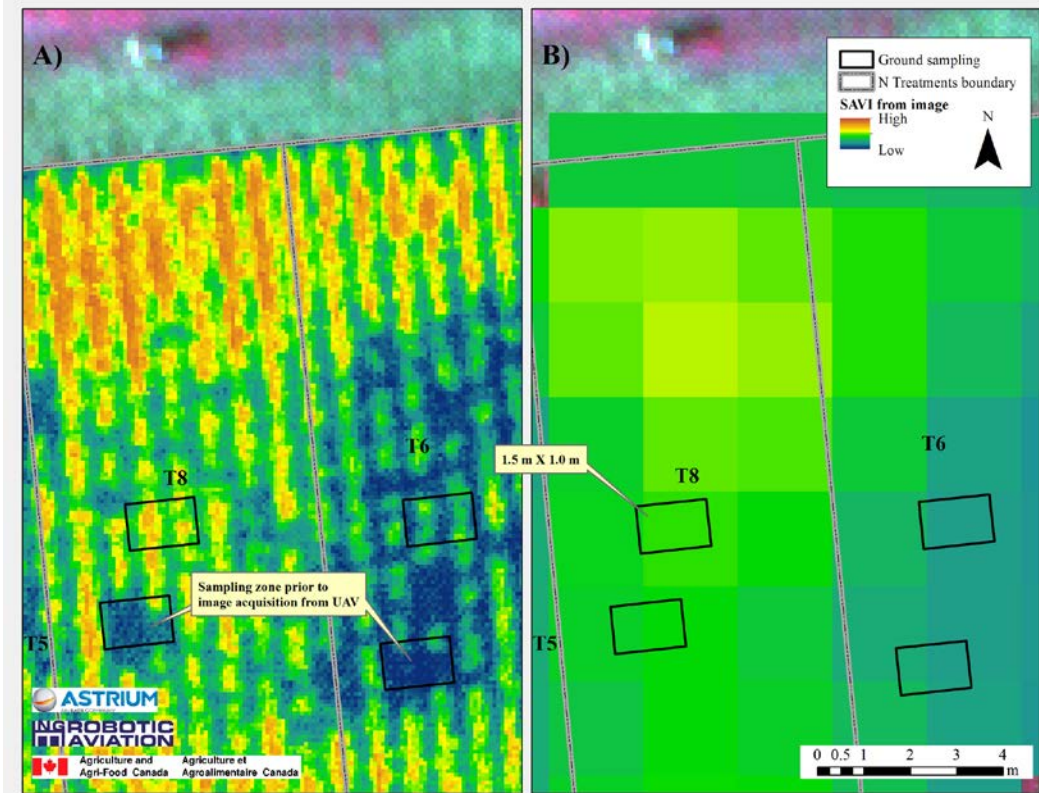
Figure 4. Visual representation of the pixels contained in the ground sampling zone forthe Mini-MCA image (A) and the Pléiades-1 image (B).
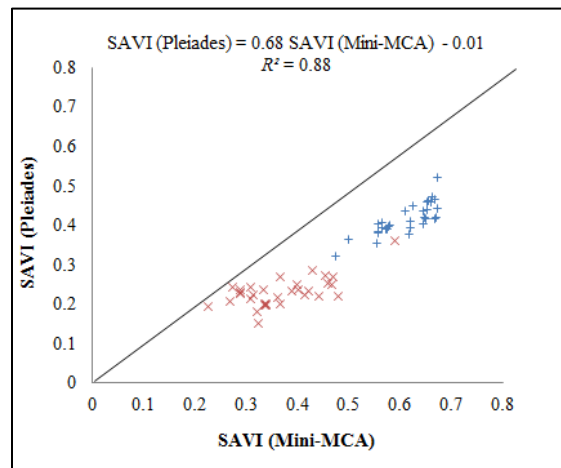

Figure 5. Relationship between the Soil-Adjusted Vegetation Index (SAVI) from satellite imagery (Pléiades-1B) and the SAVI from from the unmanned aerial vehicle imagery (Mini-MCA).

Figure 6 shows a representation of the plots in the Field 56-64 as seen from the Mini-MCA imagery. Differences in the SAVI values due to the sowing date are clearly apparent in both images. A line with higher SAVI values is visible particularly in the middle and on the north and south borders of Sowing 2, in the

upper (64, irrigated) and the lower (56, not irrigated) parts of the field, respectively. These linear patterns were traced back to the presence of tile drains and were much more evident in the Mini-MCA than in the Pléiades-1B imagery (not shown) owing to the higher spatial resolution of the former. It is apparent on the Fig. 6 that the presence of tile drains had a favorable effect on the crop at an early stage of growth, probably by removing the excess water, particularly in the upper field (64) characterized by fine soil textures. Lelong et al. (2008) showed how the fine spatial resolution was able to locate a transition pattern between two N fertilization treatments sprayed on a wheat trial.
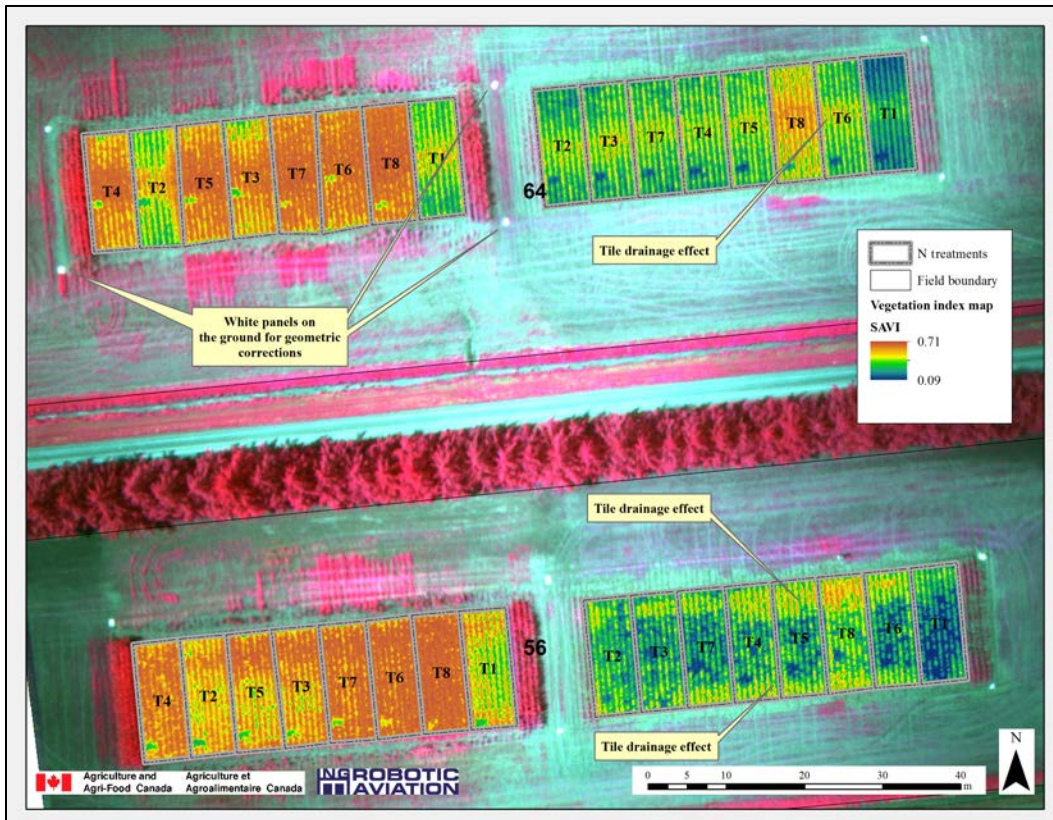

Figure 6. Representation of the plots in the Field 56-64 showing the variability in the SAVI values and the tile drainage effect.

Figure 7 presents the results of the Mini-MCA image segmentation. Pixels representing soil or shadow were masked in order to extract only those containing pure vegetation spectral characteristics. This segmentation was done to examine the potential benefit of imagery at a high spectral resolution in comparison with imagery at a coarser (satellite-based) resolution for obtaining biophysical descriptors that are better correlated to ground-truthing data.
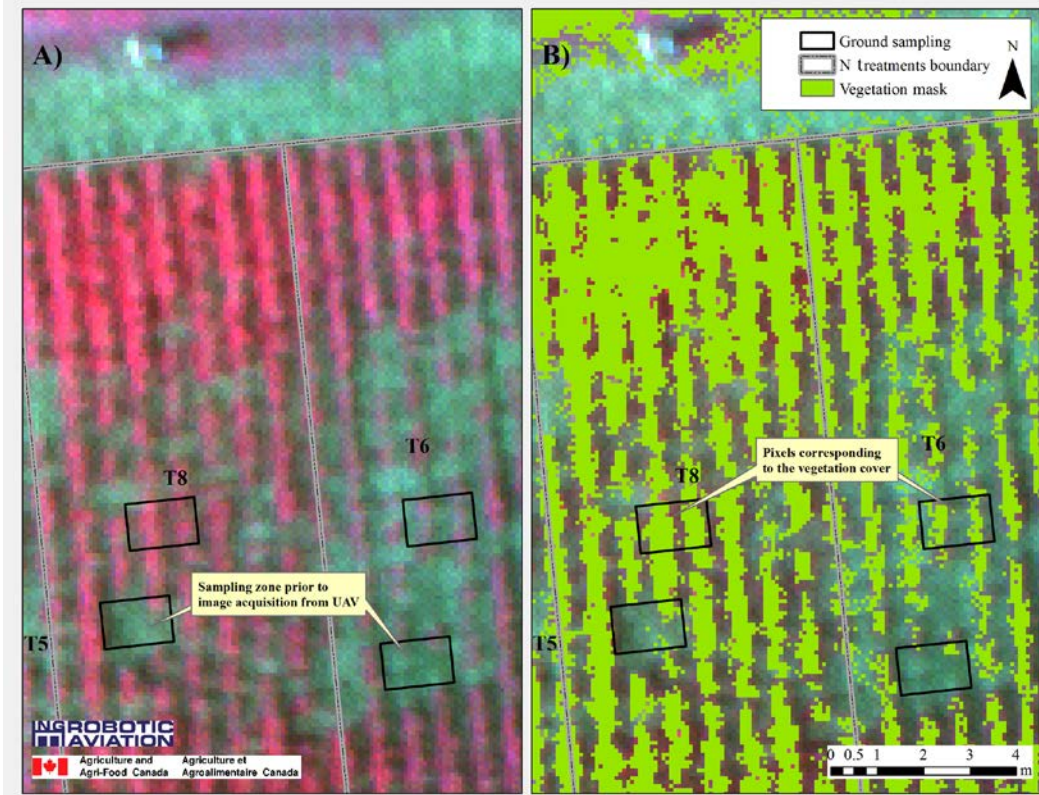
Figure 7. Result of image segmentation showing the selection of pure endmembers of leaves. N, nitrogen; UAV, unmanned aerial vehicle.

Figure 8 shows the relationships between fresh biomass and the SAVI from Pléiades-1B and from the Mini-MCA, without or with image segmentation. The SAVI from Pléiades-1B showed a steeper relationship with fresh biomass, ranging from about 0.15 to 0.5. The SAVI from the Mini-MCA was better spread out than the SAVI from Pléiades-1B between low and high SAVI values. The SAVI from the Mini-MCA ranged from about 0.2 to 0.7 without segmentation, and from about 0.27 to 0.67 with segmentation.
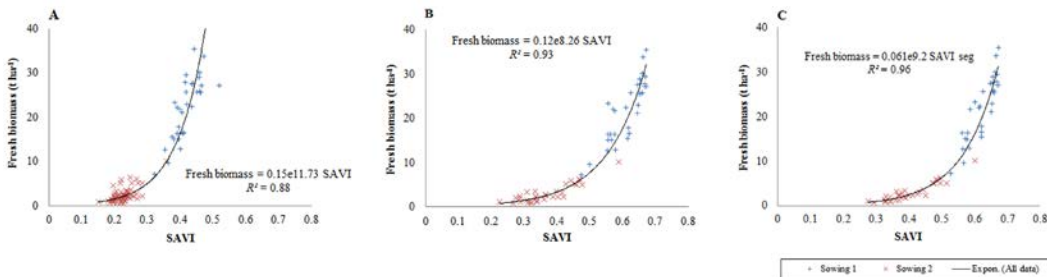

Figure 8. Relationships between fresh biomass and the the Soil-Adjusted Vegetation Index (SAVI) from Pléiades-1B (A), from the Mini-MCA without image segmentation (B), and from the Mini-MCA after image segmentation (C).

Hunt et al. (2010) reported a linear relationship between green NDVI and LAI ($R^2 = 0.85$ for $0 < LAI < 2.7$). Figure 9 shows the exponential relationships

between LAI and SAVI from Pléiades-1B or from Mini-MCA, without or with image segmentation. As for fresh biomass (Fig. 8), SAVI from Pléiades-1B showed a steeper relationship with LAI and a narrower range than the SAVI from the Mini-MCA which was better spread than Pléiades-1B between low and high SAVI values, particularly without segmentation.
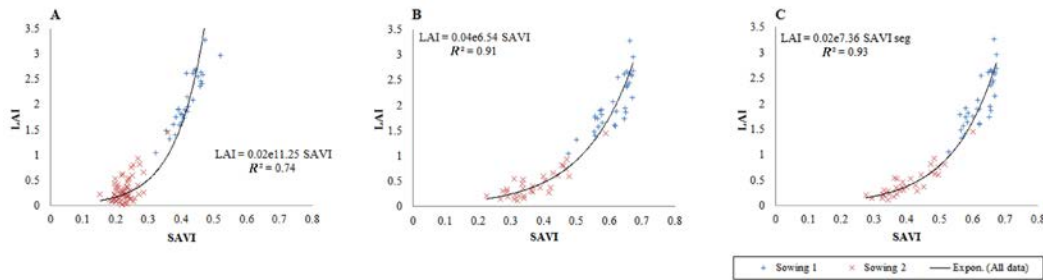

Figure 9. Relationships between leaf area index (LAI) and the Soil-Adjusted Vegetation Index (SAVI) from Pléiades-1B (A), from the Mini-MCA without image segmentation (B), and from the Mini-MCA after image segmentation (C).

The evaluation of chlorophyll status was limited to the Mini-MCA imagery since Pléiades-1B did not offer the required waveband in the red edge for TCARI/OSAVI estimation (Fig. 10). Berni et al. (2004) reported at least as good estimates from a low-cost UAV system carrying a thermal and multispectral imaging payload as from traditional manned airborne sensors for biophysical parameters in an agricultural context. The greater scatter of points at a low SPAD chlorophyll value was consistent with the greater influence of variable LAI in this context as found by Haboudane et al. (2002). Indeed, the relationship between SPAD chlorophyll and the TCARI/OSAVI was less scattered for Sowing 1 (higher and more uniform LAI) than Sowing 2 (lower and less uniform LAI). Image segmentation (Fig. 10B) slightly improved the relationship between SPAD chlorophyll and the TCARI/OSAVI. Berni et al. (2004) estimated chlorophyll $a + b$ concentration from the TCARI/OSAVI index with a R^2 of 0.89 as compared with field measurements, after the extraction of pure tree crown regions using Mahalanobis supervised classification. Those authors concluded in favor of the capabilities of the multispectral MCA-6 camera onboard a UAV platform for estimating chlorophyll content at the crown level. Based on the present results, however, the accurate remote estimation of chlorophyll status from a corn crop at an early growth stage remains a challenge, even with pure leaf endmembers resulting from image segmentation, because of relatively low and more variable LAI values at that stage than at later ones.
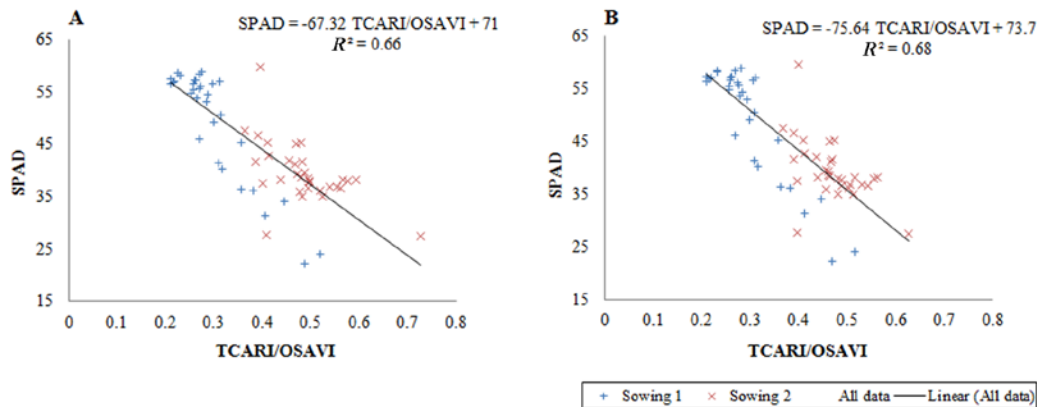
Figure 10. Relationships between SPAD chlorophyll and the TCARI/OSAVI (ratio of the Transformed Chlorophyll Absorption in Reflectance Index to the Optimized Soil-Adjusted Vegetation Index) from the Mini-MCA without image segmentation (A) and after image segmentation (B). It was not possible to calculate the TCARI/OSAVI from the Pleiades-1B image, owing to a missing waveband in the red edge.

In summary, remote N status assessment in corn is normally achieved from a vegetation index or the estimation of biophysical parameters such as biomass, LAI, and chlorophyll. This study showed that the SAVI acquired from a UAV was better correlated than imagery from a satellite to fresh biomass ($R^2 = 0.93$ for the UAV vs. $R^2 = 0.88$ for the satellite) and LAI ($R^2 = 0.91$ for the UAV vs. $R^2 = 0.74$ for the satellite). Image segmentation on the UAV imagery improved R^2 by only 0.02 to 0.03 points. Working from pure endmembers of leaves did not appear to drastically improve the relationships to biophysical parameters as suggested by Hunt et al. (2013). Image segmentation tended to narrow the dynamic range of the SAVI describing the relationships to biophysical descriptors. It also appears that the accurate remote estimation of chlorophyll status from a corn crop at an early growth stage remains a challenge, even with pure leaf endmembers resulting from image segmentation, because of relatively low and more variable LAI values at that stage than at later ones. The finer spatial resolution provided by the UAV allowed the observation of drainage effects on the vegetation which were not clearly visible in the satellite image. The UAV images required however additional care for radiometric corrections (vignetting reduction and growth targets with known references).

REFERENCES

Berni, J.A.J., P.J. Zarco-Tejada, L. Suárez and E. Fereres. 2009. Thermal and narrowband multispectral remote sensing for vegetation monitoring from an unmanned aerial vehicle. IEEE Trans. Geosci. Remote Sens. 47: 722-738.

Bouroubi, M.Y., F. Cavayas and N. Tremblay. 2010, Les corrections radiométriques des images multispectrales et leur importance pour la

fiabilité des applications de la télédétection, Éditions Universitaires Européennes, Saarbrücken, Germany, May 2010. ISBN 978-613-1-50059-6.

Haboudane, D., J.R. Miller, N. Tremblay, P.J. Zarco-Tejada and L. Dextraze. 2002. Integrated narrow-band vegetation indices for prediction of crop chlorophyll content for application to precision agriculture. Remote Sens. Environ. 81: 416-426.

Hunt Jr, E.R., W. Dean Hively, S.J. Fujikawa, D.S. Linden, C.S.T. Daughtry and G.W. McCarty. 2010. Acquisition of NIR-green-blue digital photographs from unmanned aircraft for crop monitoring. Remote Sens. 2: 290-305.

Hunt Jr, E. R., Daughtry, C. S. T., Mirsky, S. B. and Hively, W. D. 2013. Remote sensing with unmanned aircraft systems for precision agriculture applications, 2013 2nd International Conference on Agro-Geoinformatics: Information for Sustainable Agriculture, Agro-Geoinformatics, 2013. Fairfax, VA.

Laliberte, A.S., M.A. Goforth, C.M. Steele and A. Rango. 2011. Multispectral remote sensing from unmanned aircraft: Image processing workflows and applications for rangeland environments. Remote Sensing 3: 2529-2551.

Lamontagne, L., A. Martin, L. Grenon and J.-M. Cossette. 2001. Étude pédologique du comté de Saint-Jean (Québec). In: A. e. a. Canada, editor Bulletin d'extension #12. Laboratoire de pédologie et d'agriculture de précision, Centre de rercherche et de développement sur les sols et les grandes cultures, Sainte-Foy. p. 356.

Lelong, C.C.D., P. Burger, G. Jubelin, B. Roux, S. Labbé and F. Baret. 2008. Assessment of unmanned aerial vehicles imagery for quantitative monitoring of wheat crop in small plots. Sensors 8: 3557-3585.

Rey, C., M. P. Martín, A. Lobo, I. Luna, M. P. Diago, B. Millan and J. Tardáguila 2013. Multispectral imagery acquired from a UAV to assess the spatial variability of a Tempranillo vineyard. 9th European Conference on Precision Agriculture, ECPA 2013, Lleida, Catalonia: 617-624.

Ritchie, S.W., Hanway, J.J., Benson, G.O., 1996. How a corn plant develops. Special Report 48. Iowa State Univ., Coop. Ext., Serv., SR-48, Ames, IA. Available at http://www.biologie.uni-hamburg.de/b-online/library/maize/www.ag.iastate.edu/departments/agronomy/corntitle.html.

Rondeaux, G., M. Steven and F. Baret. 1996. Optimization of Soil-Adjusted Vegetation Indices. Remote Sens. Environ. 55: 95-107.

Zhang, C. and J. Kovacs. 2012. The application of small unmanned aerial systems for precision agriculture: a review. Precision Agriculture 13: 693-712.

ACKNOWLEDGEMENTS